Perturbed ion sites in Eu^{3+}:$YAlO_3$ studied by optical-rf double-resonance spectroscopy

M. Yamaguchi, K. Koyama, and T. Suemoto
Institute for Solid State Physics, University of Tokyo, Minato-ku, Tokyo 106-8666, Japan

M. Mitsunaga
Nippon Telegraph and Telephone Corporation Basic Research Laboratories, Atsugi-shi, Kanagawa 243-01, Japan
(Received 10 August 1998)

Optical excitation spectra of the Eu^{3+}:$YAlO_3$ $^7F_0 \rightarrow {}^5D_0$ transition were obtained for Eu^{3+} (0.1, 0.01, 0.001 mol %) at about 2 K. Optical excitation spectra showed more than 60 weak satellite lines spreading over some 400 GHz regardless of the Eu^{3+} concentration. From the dependence of the normalized area on concentration of Eu^{3+}, these satellite lines are ascribed to the sites differently perturbed by defects or the other Eu^{3+} ions. For the main and some satellite lines of 0.1 mol % Eu^{3+}, optical-rf (radio frequency) double-resonance spectra of the $^7F_0$ ground state have been measured. We measured hyperfine splitting frequencies δ_{RF} for given optical frequencies E_{op}, and could map site distribution on rf-optical frequency axes. In the inhomogeneous broadening for both the main and satellite lines, we found that the plot of δ_{rf} vs E_{op} had a gradient of $+10$ kHz/GHz. This finding can be explained by the *J*-mixing effect. We also obtained several rf resonance frequencies for an optical frequency at many satellites and even at valleys. From these results we can identify the sites which cannot be distinguished by a simple optical measurement. [S0163-1829(99)08913-4]

I. INTRODUCTION

The nature of inhomogeneous broadening in the optical-absorption lines of rare-earth ion-doped crystals has been studied by using spectral holeburning and optical-rf (radio frequency) double-resonance techniques for the main and some satellite lines.[1–4] These techniques are very useful to overcome the resolution limit imposed by the inhomogeneous broadening. Holeburning by using optical pumping of hyperfine sublevels has been observed in several rare-earth ions and hyperfine splittings have been obtained from the analysis of antiholes and sideholes. However, this method sometimes encounters problems in the analysis of the spectra because of complicated overlapping of the sidehole and antihole structures. To measure the hyperfine levels, optical-rf double-resonance experiment is more useful, because this technique has the advantage that the splittings are directly obtained by rf resonance free from the overlapping problem. Hyperfine splittings of trivalent europium have been measured by optical-rf double-resonance technique as previously reported for Eu^{3+}:$YAlO_3$,[5,6] Eu^{3+}:CaF_2,[7] $EuVO_4$,[1] $EuAsO_4$.[2]

In this paper, we report on the results of high-resolution excitation spectra in Eu^{3+}(0.1, 0.01, 0.001 mol %):$YAlO_3$ where we are able to resolve differently perturbed ion sites. Next, we show the distribution of the hyperfine splittings in the ground state $^7F_0$ as a function of position in the optical line in the 0.1 mol % sample. We use optical-rf double-resonance techniques to identify sites which cannot be distinguished from a simple optical spectra.

II. EXPERIMENT

The yttrium orthoaluminate $YAlO_3$ single crystals doped with trivalent Eu grown by the flux method were provided by Tokin Inc. $YAlO_3$ has a perovskitelike crystal structure with an orthorhombic distortion (i.e., of the $GdFeO_3$-type structure) and belongs to the Pnma(D_{2h}^{16}) space group.[8,9] Doped Eu^{3+} substitutes for the Y^{3+} which has the site symmetry of $C_s(C_{1h})$ containing only one mirror plane. Samples of concentrations 0.1, 0.01, and 0.001 mol % were used in our experiment. Typical sample dimensionals were $5\times5\times15\,\mathrm{mm}^3$.

A frequency stabilized ring dye laser (Coherent CR699-21 with a frequency jitter of 5 MHz) pumped by an argon ion laser was used for excitation. Absolute frequencies were measured with a Burleigh WA-1000 wavemeter, giving an absolute accuracy ±0.5 GHz. An amplitude stabilized laser beam was focused to a 1 mm beam diameter within the sample in the helium cryostat. The sample was directly immersed in superfluid liquid helium at about 2 K. The measurements of excitation spectra were carried out by exciting $^7F_0 \rightarrow {}^5D_0$ absorption band and monitoring the red fluorescence emission arising from the transition $^5D_0 \rightarrow {}^7F_2$ by a photomultiplier tube with a color filter and an interference filter (Fig. 1 inset).

We studied hyperfine splittings of Eu^{3+} 0.1 mol % using the optical-rf double-resonance technique for some satellite lines, as well as for the main line, for which double-resonance experiments have been reported.[5,6] For optical-rf double-resonance experiments, the sample was placed inside a small coil connected to an rf generator with a 6W-power amplifier. The amplitude of the rf field was estimated to be about 1.5 G. The sample was continuously irradiated by the laser at a fixed frequency to saturate the optical transition between $^7F_0 \rightarrow {}^5D_0$, with a power of 100 mW. The rf field was applied to the sample and the rf frequency was scanned. When the rf frequency becomes resonant to one of the hyperfine splitting in the ground state, the rf induces magnetic dipole transition between the hyperfine levels. This results in

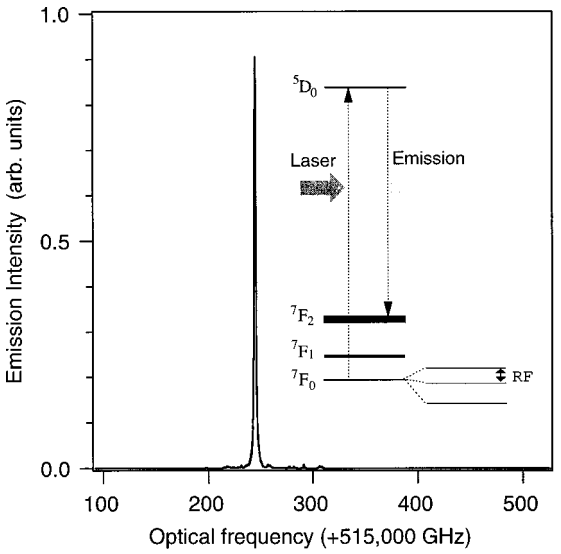

FIG. 1. Excitation spectrum of Eu^{3+} (0.1 mol %):$YAlO_3$ at about 2 K. The $^7F_0$-$^5D_0$ absorption band was excited and the $^5D_0$-$^7F_2$ fluorescence of 615 nm was monitored. The inset shows energy levels of Eu^{3+}.

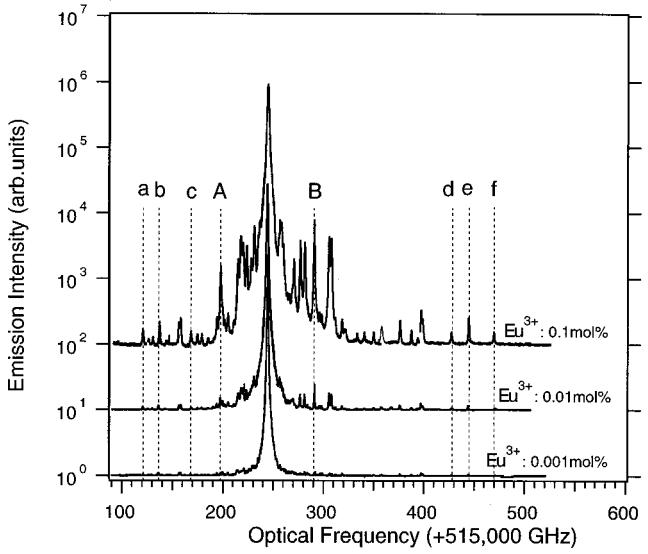

FIG. 2. Logarithmic display of the excitation spectrum of Eu^{3+} (0.1, 0.01, 0.001 mol %):$YAlO_3$ showing the weak satellite lines.

a large enhancement in optical absorption and, therefore, in substantially increased fluorescence.

III. RESULT AND DISCUSSION

A. High-resolution excitation spectrum

Figure 1 shows an excitation spectrum observed in the 581.6 nm absorption band ($^7F_0 \rightarrow {}^5D_0$) of Eu^{3+}(0.1 mol%):$YAlO_3$. This spectrum is regarded as an absorption spectrum of the Eu^{3+}. A sharp main line and very weak satellite lines smaller than 1% of the main peak intensity were observed.

Shown in Fig. 2 is a logarithmic display of the excitation spectra in which we can see the satellite structures more clearly. Such satellite lines have been frequently observed in crystals doped with rare-earth ions, for example $Nd^{3+}LaCl_3$,[10,11] Pr^{3+}:$LaCl_3$,[12] Pr^{3+}:LaF_3,[13,14] Pr^{3+}:$LiYF_4$,[15] and Eu^{3+}:Y_2O_3,[16,17] and attributed to the rare-earth ions perturbed by impurities or defects or other rare-earth ions. The satellite lines were also observed in samples with lower Eu^{3+} concentration (0.01, 0.001 mol %) and all the energy positions of these lines were in agreement with those of the 0.1 mol % sample except for one satellite line at 515 368.0 GHz which was observed only in the 0.1 mol %sample.

In the following we label some of these satellite lines by *A, B, a, b, c, d, e,* and *f* as indicated in Fig. 2. The observed lines are inhomogeneously broadened. The homogeneous linewidth is far smaller and has been established to be of the kHz order in this system.[18] The origin of the inhomogeneous linewidth of the isolated line is considered to be the averaged perturbation from numerous defects and other Eu^{3+} ions at relatively long distances. Table I shows the Eu^{3+} concentration dependence of the linewidth of the main and the labeled satellite lines. The satellite lines have nearly the same linewidth for the same Eu^{3+} concentration. The linewidth of the satellite lines decrease with decreasing Eu^{3+} concentration. This is because the averaged perturbation from other Eu^{3+} ions is less when there is larger distances between the Eu^{3+} ions in the lower concentration samples. The main peak shows the most pronounced concentration dependence. The linewidth of the main line in Eu^{3+}0.1 mol % is significantly larger than that of the satellites. On the other hand, the linewidth of the main peak for the 0.001 mol % sample becomes almost the same as that of the satellites. The satellites at frequencies far from the main peak appear as isolated peaks, while a large number of satellites pile up on both sides of the main peak resulting in an extra broadening. The above finding show that the pileup effect is practically absent for the lower concentration.

Figure 3 shows the Eu^{3+} concentration dependence of the normalized area of the satellite peaks. The normalized area is defined as the satellite area divided by the total area of the excitation spectrum. On the assumption that transition probabilities of all lines are the same, the normalized area of a

TABLE I. Dependence of the inhomogeneous linewidth on the concentration of Eu^{3+} for the main and satellite lines labeled in Fig. 2.

Eu^{3+}-concentration (mol %)	Inhomogeneous linewidth (GHz)								
	Main	*a*	*b*	*c*	*d*	*e*	*f*	*A*	*B*
0.1	1.82	1.19	1.22	1.27	1.21	1.19	1.20	1.17	0.88
0.01	1.05	1.01	0.96	1.01	0.96	1.05	1.30	1.19	0.65
0.01	0.72	0.67	0.75	0.66	0.84	0.70	0.89	0.79	0.48

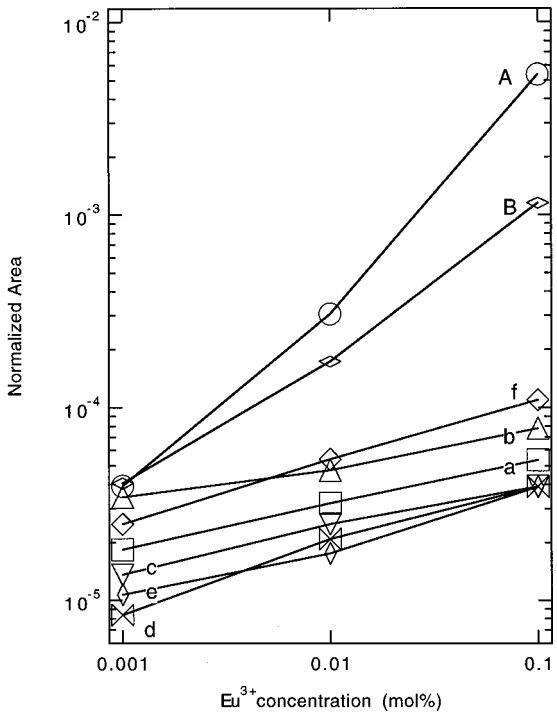

FIG. 3. Dependence of the normalized area on the concentration of Eu^{3+}. *A, B, a, b, c, d, e,* and *f* are the satellite lines labeled in Fig. 2. In *A* and *B* satellite lines, the normalized area is nearly proportional Eu^{3+} concentration. In $a-f$ satellites, the normalized area has a very weak concentration dependence.

satellite corresponds to the ratio of the number of Eu^{3+} ions in a given site to the total number of Eu^{3+} ions. In the satellite lines *A* and *B*, the normalized areas are nearly proportional to Eu^{3+} concentration. On the other hand in the satellite lines *a, b, c, d, e,* and *f*, the normalized areas have very weak concentration dependence. Most Eu^{3+} ions are spatially isolated and contribute to the main line. The satellite lines can be ascribed to Eu^{3+} ions perturbed by defects or other Eu^{3+} at relatively short distance. The satellites *A* and *B* can be assign to the Eu^{3+} ions perturbed by other neighboring Eu^{3+} ions. The number of such ions is proportional to the Eu^{3+} concentration and a liner dependence is expected. If we assume that the satellites *a, b, c, d, e,* and *f* correspond to the Eu^{3+} perturbed by the built-in defects whose number does not depend on the concentration of the Eu^{3+}, we can understand the weak concentration dependence of these peaks. We found a tendency that the peaks close to the main peak behave like *A* or *B*, and that those far from the main peak show weak concentration dependence like $a-e$. This means that the perturbation from Eu^{3+} is relatively weak compared to that from the defects.

B. Optical-rf double resonance

The Eu nucleus has a spin of $I=5/2$. The nuclear quadrupole interaction and the second-order hyperfine coupling split the $^7F_0$ ground state and $^5D_0$ excited state into three hyperfine levels ($I_z=\pm 1/2,\pm 3/2,\pm 5/2$) separated on the order of 10 MHz. The splittings are larger than the laser linewidth, so that optical excitation is only associated with one hyperfine level for an Eu^{3+}. Since natural Eu has two isotopes, ^{151}Eu(44.77%) and ^{153}Eu(52.33%), $I_z=\pm 1/2\leftrightarrow\pm 3/2$ and $I_z=\pm 3/2\leftrightarrow\pm 5/2$ transitions will give four resonance peaks in the optical-rf double-resonance spectrum. These resonances were observed at around 23, 46, 60, and 120 MHz for the main line in Fig. 4. According to the previous reports,[5,6] we interpret the 23 and 46 MHz resonances as transitions of $I_z=\pm 1/2\leftrightarrow\pm 3/2$ and $I_z=\pm 3/2\leftrightarrow\pm 5/2$, respectively in ^{151}Eu. The ratio of these two frequencies is close to 2, indicating that the asymmetry of the electric-field gradient is very small. The noisy aspect of the spectrum is due to laser jitter producing occasional jumps of the laser frequency out of the burned hole and resulting in a large fluorescence. A slight asymmetry of the line shape is due to rapid sweep of rf frequency. The slow decay is due to the hole reburned to its original depth. In Fig. 5(B), the optical-rf double-resonance spectra for the $I_z=\pm 1/2\leftrightarrow\pm 3/2$ transition of ^{151}Eu in the ground state at the main line are shown. The spectra $a-d$, respectively, are optical-rf double-resonance

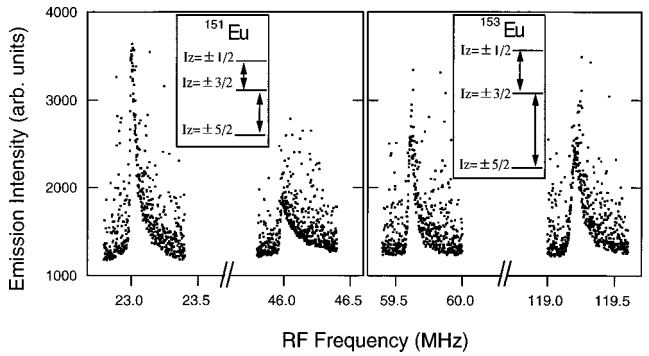

FIG. 4. Optical-rf double-resonance spectra of Eu^{3+} at main lines. The 23 and 46 MHz resonances are transitions of $I_z=\pm 1/2\leftrightarrow\pm 3/2$ and $I_z=\pm 3/2\leftrightarrow\pm 5/2$, respectively, in ^{151}Eu. The 59.6 and 119.2 MHz resonances are transitions of $I_z=\pm 1/2\leftrightarrow\pm 3/2$ and $I_z=\pm 3/2\leftrightarrow\pm 5/2$, respectively, in ^{153}Eu.

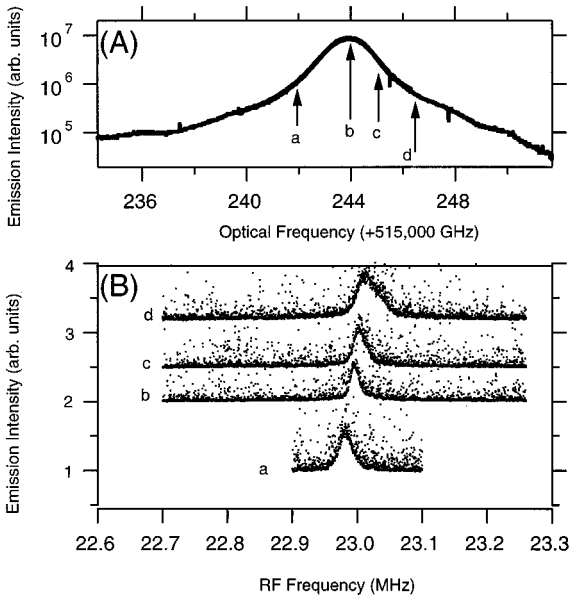

FIG. 5. (A) Excitation spectra Eu^{3+}(0.1 mol %):$YAlO_3$. (B) Optical-rf double-resonance spectra for the laser frequency tuned to *a, b, c,* and *d* labeled in (A).

spectra at the optical frequencies as indicated by the arrows in Fig. 5(A). The linewidth of the hyperfine resonances was about 20 kHz. As seen in Fig. 5(B) the peak frequencies varied linearly with the optical frequency at a rate of +10 kHz/GHz and this is in agreement with the results in Ref. 5.

In the following, we consider the shifts of hyperfine splitting in terms of the *J*-mixing effect caused by the crystal field. Although $J=2,4,6$ states admix into the $J=0$ state by the even-parity component of the crystal-field potential, we consider only the mixing of the $^7F_2$ state into $^7F_0$, because the separations of $^7F_0-{}^7F_{4,6}$ and $^5D_0-{}^5D_{2,4,6}$ are far larger than $^7F_0-{}^7F_2$. Then we can express the energy of the ground state, by using the perturbation calculation[19–22]

$$E([^7F_0])=E(^7F_0)-\frac{4}{75}\frac{1}{E(^7F_2)-E(^7F_0)}\times\sum_{q=-2}^{2}(-1)^q|B_{2q}|^2, \tag{1}$$

where B_{kq} is the *k*th-order crystal-field parameter. We make calculations by regarding the ^7F_j states in a free-ion states as pure Russell-Sanders states. The square brackets denote that the description of the states is not in terms of good quantum numbers. We may set $B_{2\pm1}=0$ and $|B_{22}|=|B_{2-2}|$, because the point symmetry of the Eu^{3+} ion site is C_s. The $^7F_0-{}^5D_0$ transition energy $E_{\rm op}$ is expressed as

$$E_{\rm op}=E(^5D_0)-E(^7F_0)+\frac{4}{75}\frac{1}{E(^7F_2)-E(^7F_0)}B_{20}^2. \tag{2}$$

Here we assumed $|B_{22}/B_{20}|^2\ll1$.[23] The transition energy is determined mainly by the crystal-field parameter B_{20}.

The hyperfine levels of each electronic state are described by a quadrupolar Hamiltonian[24]

$$H=P\left\{I_z^2-\frac{I(I+1)}{3}+\frac{\eta}{3}(I_x^2-I_y^2)\right\}, \tag{3}$$

where

$$P=\frac{3eQV_{zz}}{4I(I-1)} \tag{4}$$

and

$$\eta=\frac{V_{xx}-V_{yy}}{V_{zz}}. \tag{5}$$

Here P the effective nuclear electric quadrupole interaction constant, η is the electric-field gradient asymmetry parameter, and V_{xx},V_{yy},V_{zz} are the components of the tensor of the the electric-field gradient at the nucleus. P can be expressed as the sum of two terms,

$$P=P_{\rm latt}+P_{4f}, \tag{6}$$

where $P_{\rm latt}$ is proportional to the electric-field gradient set up by the lattice and P_{4f} is due to an electric-field gradient set up by the $4f$ electrons. The first-order contribution $P_{4f}^{(1)}$ becomes zero for $^7F_0$ in Eu^{3+}. In general, there is also P_{pq} which arises from a second-order magnetic hyperfine interaction, but these parameters are small for the Eu^{3+} ground state, so we will ignore them.[25] According to Refs. 26, 27 the parameters $P_{\rm latt}$ and $P_{4f}^{(2)}$ are given by

$$P_{\rm latt}=-\frac{3Q}{2I(2I-1)}\frac{1}{\langle r^2\rangle}\frac{1-\gamma_\infty}{1-\sigma_2}B_{20}=C_{\rm latt}B_{20}, \tag{7}$$

$$P_{4f}^{(2)}=\frac{6e^2Q}{2I(2I-1)}\langle r^{-3}\rangle(1-R_Q)\frac{\langle 20\|\alpha\|00\rangle^2}{E(^7F_2)-E(^7F_0)}B_{20}=C_{4f}^{(2)}B_{20}, \tag{8}$$

respectively. The parameters σ_2, γ_∞, and R_Q represent the shielding factor by the closed $4f$ shell, the lattice, and atomic Sternheimer shielding factors,[28] respectively. Q is the nuclear quadrupole moment, $\langle r^n\rangle$ is a concise form for $\langle 4f|r^n|4f\rangle$, the mean value of r^n for a $4f$ electron. The quantity $\langle 20\|\alpha\|00\rangle$ is a reduced matrix element of the crystal-field potential between the $J=0$ and $J=2$ states. Using these assumptions, we obtain

$$P=(C_{\rm latt}+C_{4f}^{(2)})B_{20} \tag{9}$$

from Eqs. (7) and (8). Assuming the asymmetric parameter η to be zero,[5,6] from Eq. (3), the hyperfine splitting of the $I_z=\pm1/2\leftrightarrow\pm3/2$ transition, $\delta_{\rm rf}$, is given by

$$\delta_{\rm rf}=2P. \tag{10}$$

We can obtain a relation between optical transition energy and hyperfine splitting as

$$E_{\rm op}=E(^5D_0)-E(^7F_0)+\frac{1}{75}\frac{1}{E(^7F_2)-E(^7F_0)}\times\left\{\frac{1}{C_{\rm latt}+C_{4f}}\right\}^2\delta_{\rm rf}^2 \tag{11}$$

from Eqs. (2), (9), and (10). For small change of $\delta_{\rm rf}$, Eq. (11) gives a nearly linear dependence. Furthermore, we can understand that the hyperfine splitting $\delta_{\rm rf}$ *increases* with an increase of optical frequency because the numerical factor of the $\delta_{\rm rf}^2$ term is positive. Thus, the shift in $\delta_{\rm rf}$ within a line reflects a continuous change of the electric-field gradient at the nucleus within the inhomogeneous broadening of the optical spectrum.

We measured double-resonance spectra in the range of 50 GHz including 20 satellites. Some typical spectra are shown in Fig. 6. In Fig. 6(A), two very clearly separated rf resonance lines were observed in a satellite line at about 515–291 GHz. In the optical excitation spectrum it is normally assumed that one line is associated with a single site. However, the present results clearly show that some satellite lines can correspond to overlapping contributions from two or more sites. For example, in Fig. 6(B) it can be seen that several rf resonances can even be observed at a valley in the optical spectrum. Several rf resonances are obtained at many other optical frequencies. This means that the background continuum of the luminescence spectrum is composed of many overlapped single-site peaks. The results are summarized in Fig. 7 as a mapping of resonance peaks on rf-optical frequencies axes, where the excitation spectrum is repro-

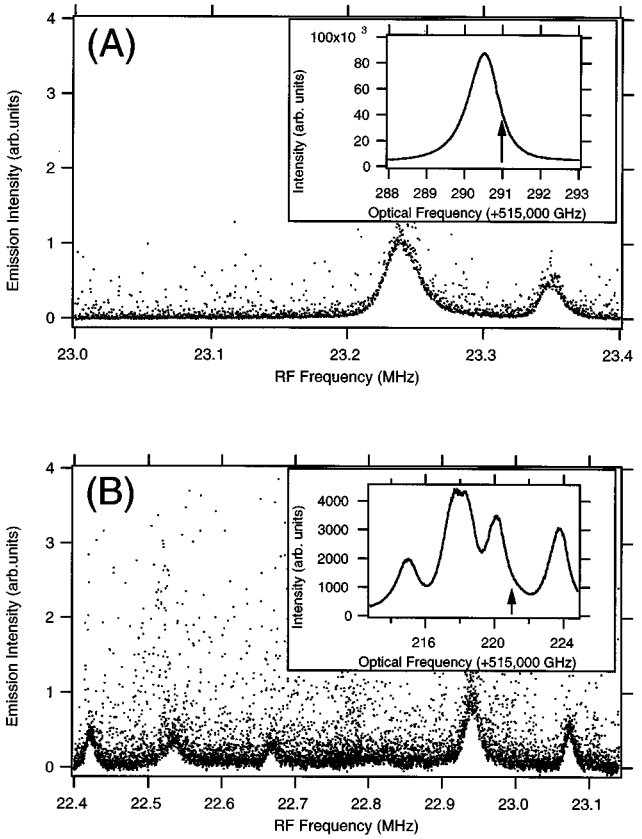

FIG. 6. Optical-rf double-resonance spectra at the optical frequency pointed by the arrow in the inset. (A) Two very clearly separated rf resonances in a satellite line. (B) Several rf resonance lines observed at a valley in the optical spectrum.

duced for a reference. The peaks which are considered to shift continuously within one optical line are traced by solid lines. In this way, it can be seen that a much larger number of sites can be identified using the optical/rf double-resonance information than can be obtained with the more conventional optical excitation. For example, in the spectral range selected in Fig. 6, up to 60 sites are identified using the hyperfine data, whereas there are only about 20 optical peaks. Thus we achieved mapping of site distribution on rf-optical frequency axes by using the double-resonance technique. In other words, these resonances reveal *hidden inhomogeneous distribution.*

Occurrence of more than two rf resonance peaks at one E_{op} cannot be explained in terms of Eq. (11), because it gives always one-to-one correspondence between δ_{rf} and E_{op}. It means that we have to consider crystal-field parameters other than B_{20} or other types of perturbations to the Eu ions in Eqs. (2) and/or (3). It is interesting to note that aside from this offset in rf resonance frequency, the variation rate of δ_{rf} vs E_{op} in each satellite line has always the same value as in the main line. This fact suggests that the nature of the inhomogeneous broadening within each line is common to all the satellites. This is consistent with the idea that the broadening is ascribed to averaged perturbation from defects or doped ions at relatively large distances.

Figure 8 shows the relationship between the rf resonance frequency ($I_z = \pm 1/2 \rightarrow \pm 3/2$) and optical frequency in a larger optical frequency range of 400 GHz. Neglecting the

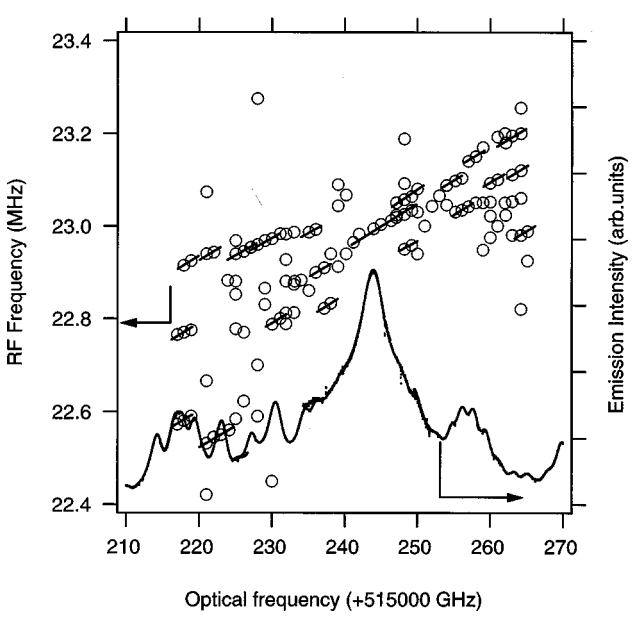

FIG. 7. Two-dimensional mapping of the site distribution (open symbols) on rf and optical frequency axes. The peak which are considered to shift within one optical line are traced by solid lines. The excitation spectrum is also shown by solid curve with an intensity scale (logarithmic) on the right.

detail, rf resonance frequency tends to increase as the optical frequency increases with roughly the same rate as the continuous shift within one satellite line. It suggests that frequency shifts at larger scale are also dominated by the crystal-field parameter B_{20}. However, there is large deviation from the relations, Eq. (11), which can be ascribed to perturbation from other crystal-field symmetries or from other mechanisms such as dipole interaction between the

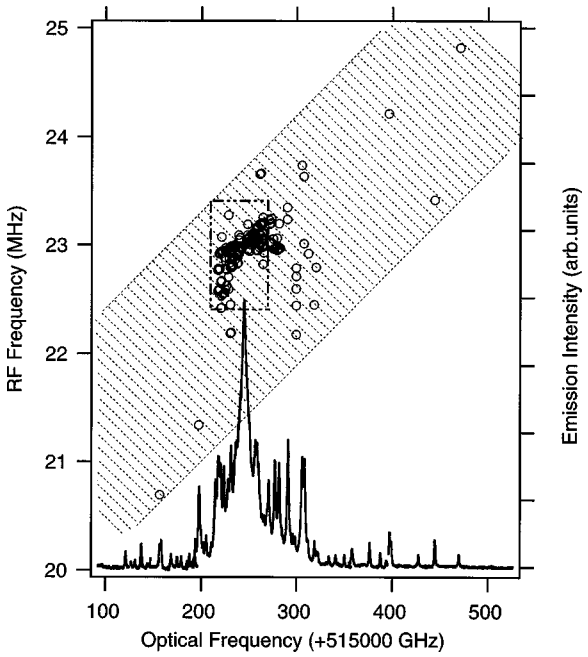

FIG. 8. The area enclosed by dotted lines shows the region investigated in Fig. 7. The slope of the shaded area corresponds to 10 kHz/GHz.

rare-earth ions. This contrasts the results for the excited state $^5D_0$ in $EuAsO_4$.[2] In this case the P parameters for various satellites were on one line.

IV. CONCLUSION

In conclusion, over 60 satellite lines spreading over some 400 GHz have been observed in optical excitation spectrum of Eu^{3+}(0.1 mol %):$YAlO_3$. These lines are ascribed to the sites differently perturbed by defects or other Eu^{3+} ions. In some satellites and in the main line, hyperfine splittings have been measured by optical-rf double-resonance technique. The rf frequency is always observed to vary at a rate of about +10 kHz/GHz within an optical line. The direction of this shift could be understood in terms of the B_{20} crystal-field parameter. Several rf resonance frequencies were often detected for one optical frequency. Thus we could map site distribution on rf-optical frequency axes. In other words, we have revealed hidden homogeneous distribution which could not be resolved by simple optical spectrum.

[1] R. L. Cone, R. T. Harley, and M. J. M. Leask, J. Phys. C **17**, 3101 (1984).
[2] R. L. Cone, M. J. M. Leask, M. G. Robinson, and B. E. Watts, J. Phys. C **21**, 3361 (1988).
[3] L. L. Wald, E. L. Hahn, and M. Lukac, J. Opt. Soc. Am. **9**, 784 (1992).
[4] M. Yamaguchi, K. Koyama, T. Suemoto, and M. Mitsunaga, J. Lumin. **76&77**, 681 (1998).
[5] L. E. Erickson and K. K. Sharma, Phys. Rev. B **24**, 3697 (1981).
[6] R. M. Shelby and R. M. Macfarlane, Phys. Rev. Lett. **47**, 1172 (1981).
[7] A. J. Silversmith, A. P. Radlinski, and N. B. Manson, Phys. Rev. B **34**, 7554 (1986).
[8] R. Diehal and G. Brandt, Mater. Res. Bull. **10**, 85 (1975).
[9] S. Geller and E. A. Wood, Acta Crystallogr. **9**, 563 (1956).
[10] G. A. Prinz and E. Cohne, Phys. Rev. **165**, 335 (1968).
[11] N. Pelletier-Allard and R. Pelletier, J. Phys. (France) **43**, 403 (1982).
[12] W. Fricke, Z. Phys. B **33**, 225 (1979); **33**, 261 (1979).
[13] J. C. Vial, R. B. Buisson, F. Madeore, and M. Poirier, J. Phys. (France) **40**, 913 (1979).
[14] J. C. Vial and R. B. Buisson, J. Phys. (France) Lett. **43**, L339 (1982).
[15] R. B. Barthem, R. B. Buisson, and J. C. Vial, J. Lumin. **38**, 190 (1987).
[16] U. Kobler, Z. Phys. **247**, 289 (1971).
[17] U. Kobler, Z. Phys. **250**, 217 (1971).
[18] M. Mitsunaga and N. Uesugi, J. Lumin. **48&49**, 459 (1991).
[19] M. Tanaka, G. Nishimura, and T. Kushida, Phys. Rev. B **49**, 16 917 (1994).
[20] M. Tanaka and T. Kushida, Phys. Rev. B **52**, 4171 (1995).
[21] G. Nishimura and T. Kushida, Phys. Rev. B **37**, 9075 (1988).
[22] G. Nishimura and T. Kushida, J. Phys. Soc. Jpn. **60**, 683 (1991); **60**, 695 (1991).
[23] N. Karayianis, D. E. Wortman, and C. A. Morrison, Solid State Commun. **18**, 1299 (1976).
[24] M. A. Teplov, Zh. Eksp. Teor. Fiz. **53**, 1510 (1967).
[25] R. J. Elliott, Proc. Phys. Soc. London, Sect. B **70**, 119 (1957).
[26] K. K. Sharma and L. E. Erickson, J. Phys. C **18**, 2935 (1985).
[27] L. E. Erickson, Phys. Rev. B **34**, 36 (1986).
[28] R. G. Barnes, R. L. Mössbaour, E. Kankeleit, and J. M. Poindexter, Phys. Rev. **136**, A175 (1964).